# Flow control of micro-ramps on supersonic forward-facing step flow*

Qing-Hu Zhang(张庆虎)[1,†], Tao Zhu(朱涛)[1], Shihe Yi(易仕和)[2], and Anping Wu(吴岸平)[1]

[1] *Hypervelocity Aerodynamics Institute of China Aerodynamics Research and Development Center, Mianyang* 621000, *China*
[2] *College of Aerospace Science and Technology, National University of Defense Technology, Changsha* 410073, *China*

(Received 20 September 2015; revised manuscript received 29 November 2015; published online 31 March 2016)

The effects of the micro-ramps on supersonic turbulent flow over a forward-facing step (FFS) was experimentally investigated in a supersonic low-noise wind tunnel at Mach number 3 using nano-tracer planar laser scattering (NPLS) and particle image velocimetry (PIV) techniques. High spatiotemporal resolution images and velocity fields of supersonic flow over the testing model were captured. The fine structures and their spatial evolutionary characteristics without and with the micro-ramps were revealed and compared. The large-scale structures generated by the micro-ramps can survive the downstream FFS flowfield. The micro-ramps control on the flow separation and the separation shock unsteadiness was investigated by PIV results. With the micro-ramps, the reduction in the range of the reversal flow zone in streamwise direction is 50% and the turbulence intensity is also reduced. Moreover, the reduction in the average separated region and in separation shock unsteadiness are 47% and 26%, respectively. The results indicate that the micro-ramps are effective in reducing the flow separation and the separation shock unsteadiness.

**Keywords:** flow control, micro-ramps, separated flows, flow imaging

**PACS:** 47.85.L–, 47.32.Ff, 47.80.Jk, 47.80.Cb **DOI:** 10.1088/1674-1056/25/5/054701

## 1. Introduction

Shock wave/boundary layer interactions (SWBLIs) have been the subject of experimental and computational research for decades owing to their practical importance in many aircrafts involving transonic or supersonic flows.[1,2] Sufficiently strong interactions can cause unstable separation and result in unsteady pressure and heat loads. Therefore, flow control strategies have been investigated to reduce the harmful effects by the SWBLIs. Although the conventional bleeding techniques have been widely used in SWBLIs control, there are some drawbacks such as high drag and mechanical complicity.[3,4] The micro vortex generators (MVGs) with a height lower than boundary layer thickness have the merits of lower drag and physical simplicity and are considered to be a hopeful alternative for bleeding techniques. In recent years, MVGs have attracted widespread attention for their promising utility in delaying separation caused by SWBLIs.

The MVGs are designed to introduce pairs of counter-rotating streamwise vortices and these flow structures can improve the characteristics of the boundary layer, which are beneficial to reduce flow separation.[5,6] The micro-ramp is one type of MVGs. Anderson *et al.*[7] used numerical simulations to determine optical designs of the micro-ramp and their results show that the micro-ramps are structurally highly robust and very affordable. Babinsky *et al.*[8] experimentally investigated the flow control ability of micro-ramps with various ramp heights. They found that the field downstream of the micro-ramp was dominated by two counter-rotating primary vortices that act to entrain high-momentum fluid from the outer regions of the boundary layer toward the surface.

Blinde *et al.*[9] used stereoscopic particle image velocimetry (PIV) to investigate the effects of the micro-ramps on SWBLIs. Different from the results of Babinsky, they found that the micro-ramps generate individual vortex pair packets downstream of their vertices, which act like longitudinal streamwise vortex pairs in a time-average view. Subsequently, Sun *et al.*[10,11] showed that the ring vortices were very important for the SWBLIs control. Due to the debates on the flow topology, the fine flow structures of the micro-ramps' control on SWBLIs need further investigation.

The reduction in the separation length and flow unsteadiness is an important aspect of the micro-ramp control. The results of Blinde *et al.*[9] show that the probability of reversed-flow occurrence is reduced by 20% to 30% and the shock motion amplitude is reduced by about 20%. Verma *et al.*[12] conducted experimental studies to control shock unsteadiness in a 24° compression ramp using MVGs. Their results show that it helps to alleviate the fluctuations of the separation shock as well as the fluctuating pressure loads in the intermittent region of separation. Very recently, Giepman *et al.*[13] investigated the influences of micro-ramp size and location on its effectiveness for SWBLIs control. Typical reductions in the average separation region 87% and shock unsteadiness 51% were recorded in their study.

Shock wave/boundary layer interactions for a forward-facing step (FFS) play an important role in both fundamental research and many practical applications.[14,15] In the present

*Project supported by the National Natural Science Foundation of China (Grant Nos. 11172326 and 11502280).
†Corresponding author. E-mail: zhang_qinghu@163.com
© 2016 Chinese Physical Society and IOP Publishing Ltd 

study, the flow control of micro-ramps on supersonic flow over an FFS is experimentally investigated using nano-tracer planar laser scattering (NPLS) and PIV techniques. The rest of the present work is arranged as follows. In Section 2, the flow facility and NPLS technique are described in detail. The flow imaging and control effects of the micro-ramps on supersonic FFS flow are given in Section 3. Lastly, conclusions are made in Section 4.

## 2. Experimental setup

### 2.1. Flow facility

The experiments were performed in a supersonic low-noise wind tunnel at Mach number 3 (Fig. 1). The total temperature $T_0$ is 300 K and the total pressure $P_0$ is 101 kPa. The experimental parameters including Mach number $Ma_\infty$, unit Reynolds number $Re$, and the flow velocity $U_\infty$ are given in Table 1. The dimensions of the test section are 120 mm in height, 100 mm in width, and 250 mm in length. The testing model for the FFS is $h_f = 10$ mm in height ($\delta/h_f = 1.02$, $\delta$ is the undisturbed turbulent boundary layer thickness), and 100 mm in width. Note that the width of the model is the same as that of the test section; therefore, the flow field at mid-span can be considered as two-dimensional (2D). The testing model is placed on a flat-plate. The micro-ramp in the present experiments has a height $h = 4$ mm (i.e., 39.2% $\delta$), with a wedge half angle $\alpha = 24^\circ$ and a chord length $c = 7.2h$. It is scaled to Anderson's specification, as shown in Fig. 2. An array of three micro-ramps are placed ahead of the testing model, with the spanwise space (the distance between two micro-ramps' center line) $s = 7.5h$, as shown in Fig. 3. The center line of the array is aligned with the center line of the flat-plate. The distance between the trailing edge of the micro-ramps and the leading edge of the FFS is 70 mm.



**Fig. 1.** Mach 3 low-noise wind tunnel.

**Table 1.** Experimental parameters.

| $Ma_\infty$ | $T_0$/K | $P_0$/kPa | $Re$/m$^{-1}$ | $U_\infty$/ms$^{-1}$ |
|---|---|---|---|---|
| 3.0 | 300 | 101 | $7.5\times10^6$ | 620 |

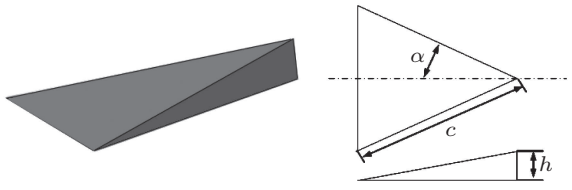



**Fig. 2.** Geometry of Anderson's micro-ramp ($h = 4$ mm, $c = 7.2h$, $\alpha = 24^\circ$).

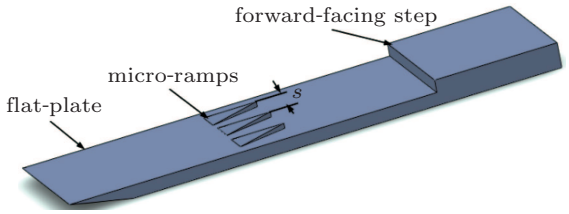



**Fig. 3.** Schematic of experimental setup.

### 2.2. NPLS and PIV technique

The NPLS is an optical flow visualization technique based on Rayleigh scattering, which uses the nanoparticles as tracer particles.[16] It has been used to investigate the supersonic mixing layer, boundary layer, compression ramp, aero-optics, and so forth.[17–19] As shown in Fig. 4, the NPLS system is composed of a nano-particle generator, a dual-cavity Nd:YAG laser, an interline transfer double-exposure CCD camera, a synchronizer, and a computer. The laser with 500 mJ pulsed energy at the wavelength of 532 nm and 8 ns pulse duration is used as a light source. The laser beam is transformed into a uniform light sheet with the thickness less than 0.5 mm by a set of cylindrical lenses. The flow is imaged using an interline transfer CCD camera with the resolution of 2048×2048 pixels. The PIV system shares the same nano-particle generator with NPLS system. Planar PIV measurements are carried out to capture the instantaneous and average velocity fields.

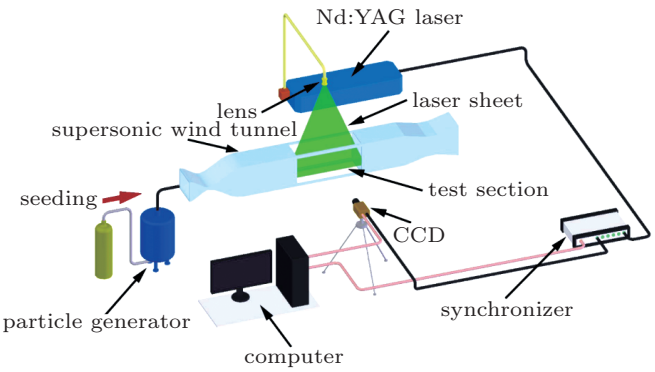



**Fig. 4.** Schematic diagram of NPLS system.

## 3. Results and discussion

### 3.1. Flow visualization

Instantaneous images of Mach 3 turbulent flow over the FFS without and with micro-ramps are shown in Fig. 5. The coordinates' origin $x = 0$ is located at the leading edge of the FFS and the coordinates of the trailing edge of the micro-ramps are $x = -70$ mm. In Fig. 5(a), the shock wave $S_1$ is the separation shock; the incoming boundary layer exhibits small hierarchy structures and has been already fully developed turbulence. In Fig. 5(b), the shock waves $C_2$ and $C_3$ are generated by the micro-ramps; the separation shock $C_1$ is distorted by

the large-scale vortex structures. Compared with Fig. 5(a), the flow structures are greatly altered in Fig. 5(b). It can be seen that the typical boundary layer is replaced by the micro-ramp's wake flow, which has a larger scale than that of the incoming boundary layer. Close to the micro-ramp's trailing edge, the flow structures exhibit a fairly darker strip, which is a slice of the micro-ramp's wake. The dark zones correspond to cross sections of the ramps' wakes which maintain an approximate round shape. The wake's interior displays a particular structure with lower luminance that appears to be the vortex cores of the primary counter-rotating vortex pair.[17] However, after a length of about $4\delta$ (at about $x = -30$), it is replaced by a new large-scale vortex, which is characteristic of intermittent large-scale structures and can survive downstream the FFS.

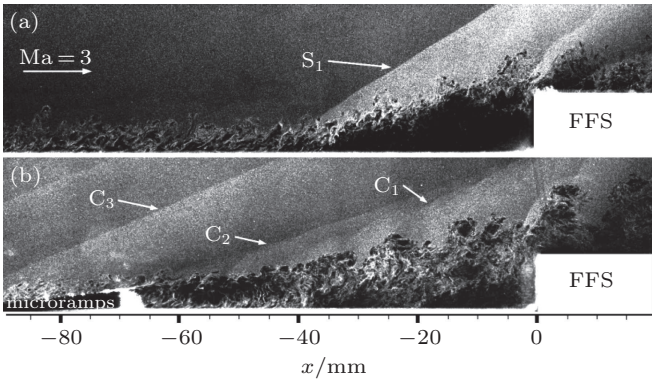



**Fig. 5.** Instantaneous images of Mach 3 flow over the FFS (a) without micro-ramps and (b) with micro-ramps.

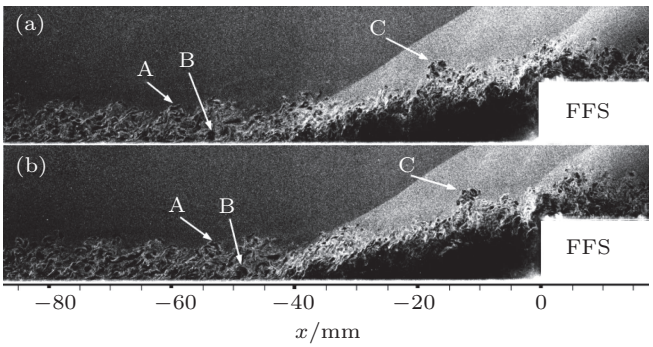



**Fig. 6.** An image pair with a 10-μs delay of Mach 3 flow over the FFS. (a) $t_1$, (b) $t_1 + 10$ μs.

Figures 6 and 7 show an instantaneous image pair with a 10 μs delay of Mach 3 flow over the forward facing step without and with the micro-ramps, respectively. In Fig. 6, after a time interval of 10 μs, the structure A in the outer part of the boundary layer only rotates clockwise for a small angle; the structure B close to the wall becomes larger and rotates anticlockwise for some angle; the structure C becomes longer in the streamwise direction. In Fig. 7, after a 10 μs delay, the structures A, B, and C have only a little change in spatial configuration but rotate clockwise for some angles. In summary, after a span of 10 μs, the large-scale structures keep most features and only move down streamwise for some distance; however, the small-scale structures have changed to some extent. The flow structures without and with the micro-ramps both have the characteristics of moving very fast and changing slowly in form.

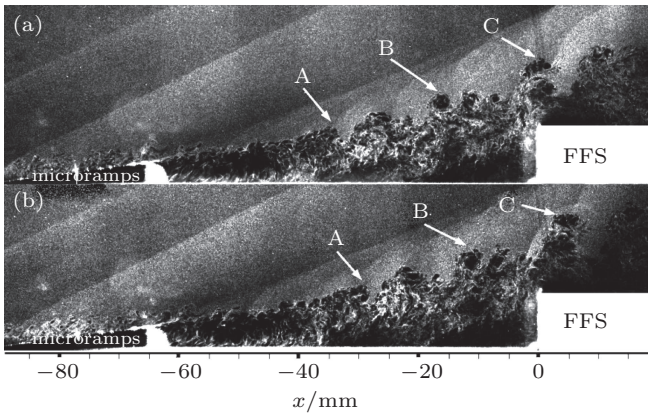



**Fig. 7.** An image pair with a 10-μs delay of Mach 3 flow over the FFS with the micro-ramps. (a) $t_2$, (b) $t_2 + 10$ μs.

Figure 8 reports a typical particle image recording of Mach 3 flow over the FFS. It can be seen that the particles are uniformly seeded. The total datasets of 500 image pairs were obtained. As a pre-processing step, the particle image was normalized using a min/max filter. The data analysis was performed using a correlation window of 32 × 16 pixels with a 50% overlap shifting, yielding a spatial resolution of 16 × 8 pixels (= 0.86 mm ×0.43 mm). Vectors' validation was accomplished by deleting vectors whose cross-correlations did not meet a sufficient signal-to-noise ratio, and deleting those whose magnitudes and directions varied too much from their nearest neighbors.

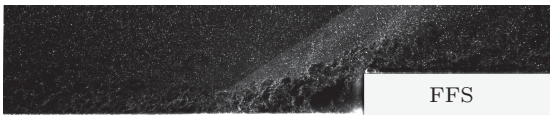



**Fig. 8.** Particle image recording of Mach 3 flow over the FFS.

Figure 9 shows the velocity topology of Mach 3 flow over the FFS with and without micro-ramps. The average velocity profiles ($u$-component) are compared in Figs. 9(a) and 9(b), while the turbulent intensities are in Figs. 9(c) and 9(d). The $U/U_\infty = 0$ line distinguishes the reversal region from the outer flow. Without the micro-ramps, the range of the reversal flow zone in streamwise direction is $3.4\delta$, while it is $1.7\delta$ with the control of micro-ramps. The reduction is 50%. The flow field contains a high-velocity outer layer (typically $U/U_\infty > 0.5$), and a low-velocity inner layer (typically $U/U_\infty < 0.5$).[17] With the control of micro-ramps, the low speed region ($0 < U/U_\infty < 0.5$) is enlarged more than that

without control. The cause is the reduction of reversal flow region and the intermittent large-scale structures induced by the micro-ramps. The reduction of reversal flow region makes the $U/U_\infty = 0$ line close to the wall. Meanwhile, the intermittent large-scale structures induced by the micro-ramps are larger than those without the micro-ramps, which make the $U/U_\infty = 0.5$ line far away from the wall. As a result, the velocity gradients in the low speed region are smaller than that without control. In addition, it results in lower turbulence level, as seen in Figs. 9(c) and 9(d). Herein, two-dimensional turbulence intensity $\mathrm{Tu} = \sqrt{u'^2 + v'^2}/U_\infty$ is adopted. From Figs. 9(c) and 9(d), it can be seen that the region for the highest turbulence intensity values is almost the same as the zone between the zero-velocity line and $U/U_\infty = 0.5$ line.

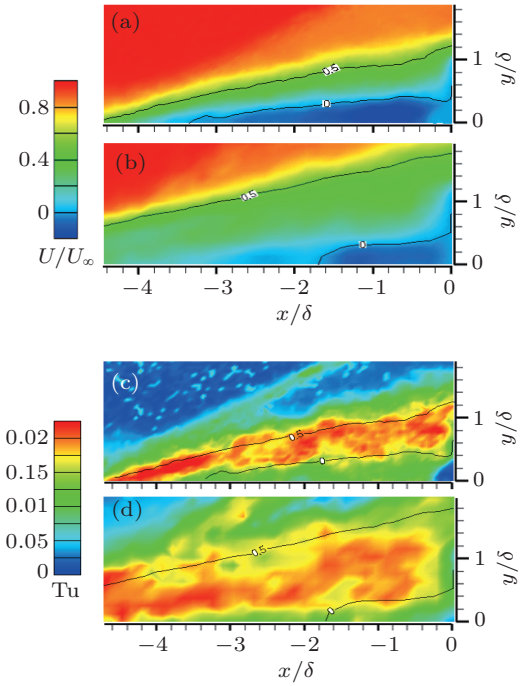



**Fig. 9.** The average streamwise velocity profiles $U/U_\infty$ (a) without and (b) with micro-ramps. Turbulent intensity $\mathrm{Tu} = \sqrt{u'^2 + v'^2}/U_\infty$ (c) without and (d) with micro-ramps. The solid black lines represent streamlines of $U/U_\infty = 0$ and 0.5, respectively.

### 3.2. Control effects

The unsteady behavior of the separation bubble is presented in Fig. 10, showing two instantaneous PIV images of Mach 3 flow over the FFS with micro-ramps. Figure 10(a) shows a small separation bubble of approximately 16 mm$^2$, while figure 10(b) presents a large separation bubble of about 102 mm$^2$. Here, the size of the separation bubble is approximately calculated by the flow reversal region within the zero-velocity line.

The local separation probability $P_{\mathrm{sep}}$ is defined as the percentage of the time reversed flow occurs at a certain point $(x, y)$. Figure 11 compares the separation probability of the FFS flow field with and without micro-ramps, here, $P_{\mathrm{sep}}$ is calculated from an ensemble of 500 PIV images. From Fig. 10, it can be seen that the flow reversal region with the control of micro-ramps is only slightly reduced compared with no control. However, the probability of encountering reversed flow at a certain point is greatly reduced, i.e., the probability of encountering reversed flow is greatly reduced, especially at some regions close to the FFS, which can be seen from the grayness value of the Fig. 11. Mean flow separation can then be defined as the point where the flow is separated for 50% of the time, so the mean separated area $A_{\mathrm{sep}}$ is calculated by integrating the 50% separation probability domain. Without the control of micro-ramps, $A_{\mathrm{sep}}$ is 91.7 mm$^2$, while it is 48.5 mm$^2$ with the micro-ramps. The reduction is 47%.

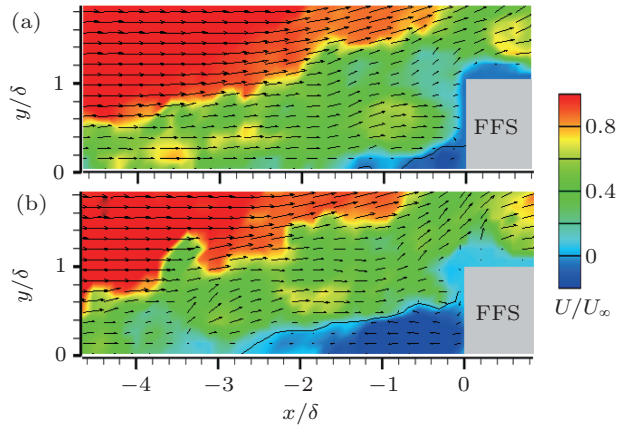



**Fig. 10.** Two uncorrelated instantaneous PIV images of the FFS flow field with micro-ramps. The solid black line shows the zero-velocity iso-line. (a) Small separation bubble. (b) Large separation bubble.

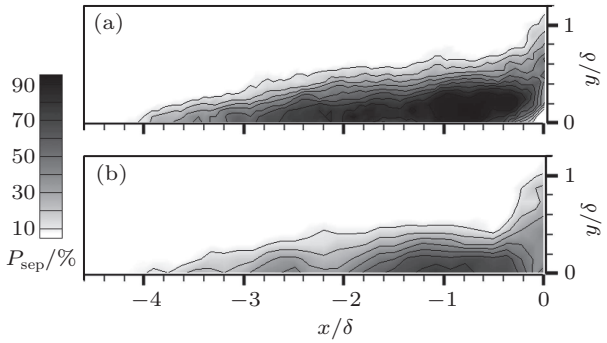



**Fig. 11.** The separation probability $P_{\mathrm{sep}}$ of the FFS flowfield (a) without a micro-ramp and (b) with micro-ramps.

Since the size of the separated bubble is correlated with the position of the separation shock,[13,20] it is expected that when the size/unsteadiness of the separated bubble decreases, the unsteadiness of the separation shock also reduces. After the shock wave, there is a great velocity gradient. Therefore, the shock position can be determined by locating the biggest velocity gradient along the $x$ direction at different wall-normal locations. In order to evaluate the unsteadiness of the separation shock, its location is calculated by finding the maximum of $\mathrm{d}V/\mathrm{d}x$ along the horizontal line $y = 3\delta$. The same procedure is repeated for the five rows of vectors above and below this line. After removing obvious edges, the separation

shock locations are obtained in a least squares fitting procedure. This linear fit is employed to calculate the shock position at $y = 3\delta$.[13] The process is repeated for all 500 images, then the separation shock unsteadiness is represented by the standard deviation $\sigma$ of shock locations $x_s$ at $y = 3\delta$. Without control of a micro-ramp, the standard deviation $\sigma(x_s)$ is 1.71, while with micro-ramps it decreases to 1.26. The reduction in separation shock unsteadiness is 26% with the control of the micro-ramps.

## 4. Conclusion

The flow control effects of the micro-ramps on Mach 3 turbulent flow over a forward-facing step was experimentally investigated in a supersonic low-noise wind tunnel using NPLS and PIV techniques. High spatiotemporal resolution flow visualization and velocity fields were captured. With the micro-ramps, the flow fields are dominated by intermittent large-scale structures generated by the micro-ramps, which can survive the downstream region of the FFS flowfield. After 10 μs, there are little changes in large-scale structures and the flow structures change slowly in form. Furthermore, the micro-ramps have almost no impact on the evolution characteristics of the flow structures. With the micro-ramps, the reduction in the range of the reversal flow zone in streamwise direction is 50%, the low speed region is greatly enlarged and the turbulence intensity is reduced. The reduction in the average separated region is 47%, which is rather close to the reduction in the streamwise scope of the reversal flow region. Moreover, the reduction in separation shock unsteadiness is 26% with the control of the micro-ramps. The results show that the micro-ramps are effective in controlling the supersonic FFS flow.

## References


[1] Gaitonde D V 2015 *Prog. Aerospace Sci.* **72** 80
[2] Sun Q, Cui W, Li Y H, Cheng B Q, Jin D and Li J 2014 *Chin. Phys. B* **23** 075210
[3] Li Q and Liu C Q 2010 *J. Aircraft* **47** 2086
[4] Huang Y, Wang X N and Huang Z B 2013 *Chin. Phys. Lett.* **30** 094702
[5] Frank K L, Li Q and Liu C Q 2012 *Prog. Aerospace Sci.* **53** 30
[6] Lee S, Loth E, Georgiadis N J and DeBonis J R 2011 *AIAA J.* **49** 97
[7] Anderson B H, Tinapple J and Suer L 2006 3*rd AIAA Flow Control Conference*, 5–8 June, San Francisco, USA, AIAA, p. 3197
[8] Babinsky H, Li Y and Ford C W P 2009 *AIAA J.* **47** 668
[9] Blinde P L, Humble R A, van Oudheusden B W and Scarano F 2009 *Shock Waves* **19** 507
[10] Sun Z, Schrijer F F J, Scarano F and van Oudheusden B W 2012 *Phys. Fluids* **24** 055105
[11] Sun Z, Scarano F, van Oudheusden B W and Schrijer F F J 2014 *AIAA J.* **52** 1518
[12] Verma S B, Manisankar C and Raju C 2012 *Shock Waves* **22** 327
[13] Giepman R H M, Schrijer F F J and van Oudheusden B W 2014 *Phys. Fluids* **26** 066101
[14] Largeau J F and Moriniere V 2007 *Exp. Fluids* **42** 21
[15] Ren H Y and Wu Y H 2011 *Phys. Fluids* **23** 045102
[16] Zhao Y X, Yi S H, Tian L F and Cheng Z Y 2009 *Sci. China Ser. E* **52** 3640
[17] Wang B, Liu W D, Zhao Y X, Fan X Q and Wang C 2012 *Phys. Fluids* **24** 055110
[18] Zhu Y Z, Yi S H, He L, Tian L F and Zhou Y W 2013 *Chin. Phys. B* **22** 014702
[19] Wu Y, Yi S H, He L, Chen Z and Zhu Y Z 2014 *Chin. Phys. B* **23** 114702
[20] Smits A J and Dussauge J P 2006 *Turbulent Shear Layers in Supersonic Flow* (2nd edn.) (New York: Springer) pp. 323–325